01 Nov 2023

Iron Oxide Ore Mineralogy and its Plant Flotation Circuits Nodal Analysis Simulation and Comparison

Ying Hou

Ahmed Sobhy
Missouri University of Science and Technology, asobhy@mst.edu

Samah Abdel Aziz

Recommended Citation

Y. Hou et al., "Iron Oxide Ore Mineralogy and its Plant Flotation Circuits Nodal Analysis Simulation and Comparison," *JOM*, vol. 75, no. 11, pp. 4771 - 4781, Springer; Minerals, Metals and Materials Society (TMS), Nov 2023.
The definitive version is available at https://doi.org/10.1007/s11837-023-06122-9

JOM, Vol. 75, No. 11, 2023
https://doi.org/10.1007/s11837-023-06122-9

TECHNICAL ARTICLE

Iron Oxide Ore Mineralogy and Its Plant Flotation Circuits Nodal Analysis Simulation and Comparison

YING HOU,[1] AHMED SOBHY ,[2,3,5] and SAMAH ABDEL AZIZ[4]

1.—School of Mining Engineering, University of Science and Technology Liaoning, Anshan 114051, Liaoning, China. 2.—School of Resources and Environmental Engineering, Shandong University of Technology, Zibo 255049, Shandong, China. 3.—Minerals Technology, Central Metallurgical Research and Development Institute, Helwan, Cairo 11421, Egypt. 4.—Faculty of science, Zagazig University, Zagazig 44519, Egypt. 5.—e-mail: a.sobhy@qq.com

Mining operations usually provide ore of varying characteristics. At the Donganshan Sintering Plant, the ore is a low-grade, complex, hard-to-separate carbonate containing iron ore, and a two-step flotation circuit was previously developed to overcome the negative impact of the carbonates on the reverse flotation process. However, with the further expansion in the mining operations, it was difficult to maintain a highly efficient flotation process. Thus, the mineral liberation analyzer (MLA) was utilized to conduct an in-depth process mineralogy investigation. MLA showed that the main useful minerals in this ore are magnetite/hematite of 45% total iron, and the main gangue mineral is quartz of 29.97%, followed by 2.55% chlorite and 1.48% ankerite with about 0.03% siderite. Accordingly, flotation circuit modification was mandatory by eliminating the direct flotation process used prior to reverse flotation. Therefore, two-step and reverse flotation circuits were balanced using nodal simulation, and the two circuits produced 48.91% and 49.45% yield, 65.03% and 65.22% total iron grade, and 70.96% and 72.08% total iron recovery, respectively. Thus, reverse flotation is comparable with two-step flotation by 0.54%, 0.19%, and 1.12% higher yield, grade, and recovery, respectively. In addition, the process flow sheet was not only simplified but it also enhanced the performance with reduced reagent consumption.

INTRODUCTION

Iron is considered the third most abundant mineral to be discovered, and it has different chemical forms. Iron oxides ore is the most abundantly available resource compared to sulfide and carbonate.[1] The majority of iron ore reserves in China are low-grade, finally disseminated, and scattered reserves.[2] The estimated national reserves are more than 20 billion tons,[3] and one-fifth of the estimated reserve is located in the Anshan region, Liaoning.[4] The overall world iron reserves exceed 170 billion tons.[5]

(Received March 20, 2023; accepted August 25, 2023; published online September 22, 2023)

Figure 1 shows that China has the largest iron production in the world, according to the US geological survey.

A large proportion of iron ore at the Donganshan processing plant, which is the largest producer of iron oxide product/concentrate in China, is low-grade, complex, difficult-to-separate carbonate-containing refractory iron ore.[6] With the development of the mining operation, the carbonate contents have increased in the iron ore at the Donganshan processing plant, which negatively affects the reverse flotation circuit efficiency.[7] In the flotation process, the behavior of the mineral floatability of the iron oxide ore constituents changes extensively as a result of the variations in the mineralogy of the ore. Furthermore, the physiochemical properties change from ore to ore, due to the nature of the valuable iron oxide ore and the associated less

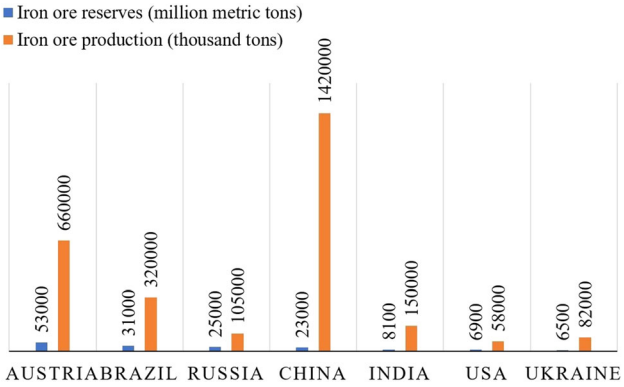

Fig. 1. The production of iron ore and reserves worldwide in 2016 based on information from the US geological survey.

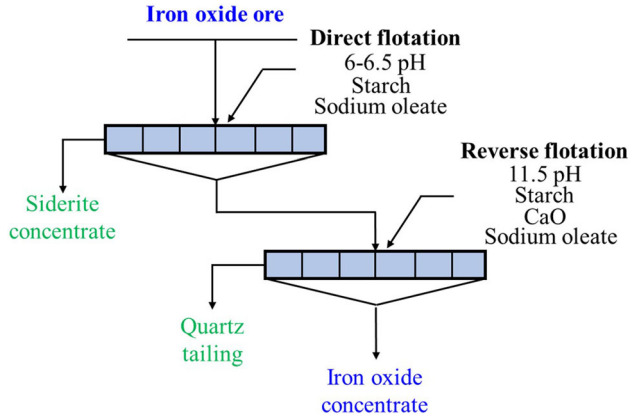

Fig. 2. Two-step flotation process developed for carbonaceous iron oxide ore.

valuable/gangue minerals, such as carbonates, sulfur, and phosphorous in various forms.[8] For the iron oxide ores, there are two flotation methods: direct and reverse. In flotation, petroleum sulfonates and fatty acids are two commonly used anionic collectors. These chemicals are structurally composed of negatively charged ionic heads and long-chain organic tails.

Usually, one flotation stage is insufficient to produce the final concentrate; thus, industrial flotation circuits are employed. These circuits are commonly utilized to remove the non-valuable from the valuable minerals as a result of their differential flotation rates. Flotation mainly exploits the difference in hydrophobicity, and is used in many industries for fine particle separation. In reverse flotation, which is the opposite of direct flotation, the gangue mineral such as quartz is floated by using a suitable flotation reagent system, while the valuable minerals such as iron oxide, remains in the slurry and is collected as a concentrate/product. In the iron industry, the reverse flotation of iron ore has been successfully employed for more than 20 years.[9]

The iron ore at the Donganshan processing plant contains mainly magnetite and hematite fine-grained particles, which are easy to lose in the flotation tailings.[6] In addition, the presence of carbonaceous minerals, mainly siderite, in the ore increased significantly with increasing of the mining depth during development, which impacted both the grade and the recovery of the iron oxide product/concentrate from the reverse flotation process.[9] The main reason behind the lower process efficiency is that siderite is softer than iron oxide and quartz minerals, which creates slimes of siderite adsorbed on the surface of the other minerals and, in consequence the floatability of the iron oxide and quartz become approximately similar to that of siderite.[9]

As a result, a suitable flotation process called two-step flotation mainly for carbonaceous iron oxide ore was developed and applied to the Donganshan iron ore.[1,9,10] The developed process is mainly divided into two stages: direct flotation at the near-neutral condition and reverse flotation under an alkaline condition, as illustrated in Fig. 2.[11–13] Thus, the siderite concentrate is floated in the first stage to eliminate its negative effects on the recovery of iron oxide in the second stage.

In addition, the flotation performance is significantly affected by the quantity of flotation reagents, which has been previously studied extensively by the authors.[14–18] Thus, in a flotation circuit, an unsuitable reagent system leads to metal loss with reduced product quality. In the direct flotation stage of iron ores, the flotation reagent system comprises pH regulators, depressants, and collectors; while, in the reverse flotation stage, the same flotation reagent system is used in addition to using activators prior to the addition of collectors.[15]

Furthermore, the chemical reagents such as starch is utilized as a depressant for iron oxide minerals, while sodium oleate is added as a collector for siderite at 6–6.5 pH value and for quartz after activation with lime at 11.5 pH. The dosages of these reagents significantly influence the separation performance of the two-step or reverse flotation circuits.

Recently, with the mining development, the original mineral properties have changed again at the Donganshan processing plant. Thus, it is worth exploring the ore properties, the possible flotation process circuits, and the associated flotation reagent systems to maximize the iron oxide quality and recovery.

Objectives

This work presents maximizing the plant efficiency and reducing the reagent consumption which increases the plant profitability, in which the iron oxide ore acquired from the Donganshan processing plant was subjected to extensive process mineralogy characterization using an Advanced Mineral Identification and Characterization System (AMICS). Also, the possible flotation circuits such as two-step

flotation and reverse flotation circuits were utilized, balanced, and optimized for comparison purposes to identify which of them has a higher separation performance in its optimum flotation plant reagent system.

Paper Organization

The structure of this article is organized as follows: "Introduction" section presents the introduction, objectives, and organization of the topic. "Materials and Methods" section introduces comprehensive details of materials, MLA sample characterization, experimental methods, and nodal analysis simulation. The results and a comparison between two-step and reverse flotation circuits are presented in "Results and Discussion" section. "Conclusions" section concludes the results and shows the efficiency of the performance of our proposed flowsheet.

MATERIALS AND METHODS

Materials

The as-received experimental sample is a representative flotation feed, which is a mixture of particles after the magnetic separation circuit from the Donganqian processing plant in Anshan, Liaoning, China. The representative sample was collected over a day, 5 gallons (c. 19 L) every 2 h. The collected samples were mixed, dried to remove the moisture contents, split into small portions of about 650 g, and sealed in plastic bags for later usage.

All the experiments were performed using the local industrial flotation chemical reagents from the Donganqian processing plant, and used as they were in the study. These chemicals which were starch, lime (CaO), and anionic TD-II, were employed as depressant, activator, and collector, respectively. HCl (15% w/w) and NaOH (15% w/w) were used for pH adjustment.

MLA Sample Characterization

For accurate characterization, 100-g representative samples were classified by sizing into three closed sizes using 74-μm and 38-μm standard sieves. The samples were homogenized by mixing, mounted in epoxy, then polished. The polished samples were subjected to carbon spray by a C-ion sputter evaporator to ensure conductivity on the sample surface.

The full characterization was carried out by conducting AMICS, which combines advanced image analysis to segment particles of mineral phases boundary, element analysis with Sigma 500, and scanning electron microscopy (SEM) for high-quality imaging of $\times$ 300 magnification, and x-ray microscopy with hybrid mode options of backscattered electrons (BSE) with the QUANTEX EDS system for advanced analytical microscopy. The measurements were performed under the following parameters: an accuracy of 0.56-μm pixels, a probe current of 10 nA, and an acceleration voltage of 20 kV for the total electron beam. The background was then epoxy resin (BSE grayscale value $<$ 35) and metal as the upper limit (BSE grayscale value $>$ 255). The BSE setup was accomplished by image grayscale calibration, and the resulting data were processed by AMICS Process software.

Experimental Methods

In the flotation circuit, laboratory flotation experiments were conducted on a representative sample of each of the streams using a temperature-controlled XFG-III flotation machine (Nanchang Jianfeng Mining Machinery Manufacturing, Jiangxi, China) with a 1.5 L cell at 35°C, 33.3% solids, and 1920 rpm rotor speed. Unless otherwise stated, direct flotation was carried out at near-neutral pH by using starch for 3 min to depress the magnetite/hematite and quartz minerals, and a TD-II commercial anionic collector to float the siderite (iron carbonate) for 2 min.

For the reverse flotation, the samples suspension pH was adjusted to 11.5 by adding pH regulators (NaOH) for 3 min, and then the starch was mixed for 3 min. Next, CaO was added for 3 min to activate the quartz to accommodate the adsorption of the TD-II commercial anionic collector for 2 min. The flotation time was kept constant at 3 min.

The whole process was carried out by using roughing, cleaning, and three scavenging flotation stages. However, in the case of the two-step flotation circuit, direct flotation was used at the beginning, followed by roughing, cleaning, and three scavenging flotation stages. All the flotation experiments were carried out under the same air flow rate and minimum froth height, so that the changes in flotation rate were mainly due to the stream properties and the flotation kinetics.

The froth was scraped manually by using a plastic blade. The concentrates and tailings from each step were dried, weighed, and analyzed for the total iron grade and recovery. The two flotation circuits were investigated and compared in terms of their chemical reagent system, and iron oxide yield, grade, and recovery.

Nodal Analysis Simulation

A nodal analysis method has been utilized to minimize the efforts and time consumed in the mass balancing of these complex circuits. In addition, it minimizes the number of streams to be analyzed, while simultaneously determining the complete mass balance and missing analysis data around the circuit and each process unit in the circuit. The nodal analysis method simply generates linear equations to solve for unknown data.

A node is a segment in the flotation circuit where the streams are either combined or separated. It can be a single unit in the flotation circuit such as a

junction (sump pump), rougher flotation, cleaner flotation, and scavenger flotation. The characteristics of the streams entering and exiting a node are identified by connection matrix, $C_{i,j}$, for node I and stream j, where each element in the matrix is represented by:

$$\begin{aligned} C_{i,j} = &+1 \text{ for stream } j \text{ flowing into the } i\text{th node} \\ &-1 \text{ for stream } j \text{ flowing out of the } i\text{th node} \\ &0 \text{ for stream } j \text{ not appearing in the } i\text{th node} \end{aligned} \quad (1)$$

Each column in the matrix must sum to equal 0, 1, or – 1 for the internal, feed, and product streams, respectively, and each row in the matrix must equal + 1 or – 1 for the junction or separator nodes, respectively.

Based on the material flow rate and component values (total iron grade) around the various nodes, the material matrix $M_{i,j}$ (Eq. 2) and component matrix $A_{i,j}$ (Eq. 3) are generated for a set of linear equations:

$$M_{i,j} = C_{i,j}B_j \quad (2)$$

$$A_{i,j} = C_{i,j}B_j a_j = M_{i,j}a_j \quad (3)$$

where Bj and a_j are the mass flow rate of the material and the component value in stream j, respectively.

Then, the Gaussian elimination method has been used to estimate the mass flow rate of each stream by selecting a minimum number of process streams (N) to be analyzed, with N is estimated by:

$$N = 2\,(F + S) - 1 \quad (4)$$

where F is the number of the feed stream to the circuit and S is the number of separators in the circuit. Then, the developed set of equations has been used to determine the complete mass balance of the whole circuit.

RESULTS AND DISCUSSION

Flotation Feed Characterization

Mineral Composition

The AMICS analysis system showed that the main valuable minerals in the plant flotation feed are magnetite/hematite minerals, and that the main gangue minerals are quartz and a wide variety of other minerals. The mineral content of each of these is shown in Table I, which shows that 62.99% of the flotation feed consists of magnetite/hematite valuable minerals, and 29.97% quartz as a gangue mineral followed by other impurities. Pulsar minerals such as chlorite (turquoise) and ankerite (iron dolomite) are about 2.55% and 1.48%, respectively. Sulfur-containing minerals are mainly yellow iron ore (pyrite), and phosphorous-containing minerals are mainly phosphorite (apatite), and their contents are 0.14% and 0.12%, respectively. The content of iron carbonate ore (siderite) is only 0.03%.

Size Distribution of Major Mineral Grains

The particle size of the flotation feed is 87.61% finer than 74 μm particle size. The particle size distribution of the main minerals in the flotation feed has been analyzed by the AMICS test system, and the results are shown in Fig. 3. The figure indicates that the particle sizes of magnetite/hematite and quartz in the flotation feed are coarser, the granularity of chlorite is finer than that of magnetic/hematite and quartz, and the particle size of iron dolomite is the finest. It can be concluded that, during grinding, magnetic/hematite and quartz are not easily ground, while chlorite and ankerite are easily ground and muddy phenomena occur, which will have a greater impact on the subsequent flotation separation.

Major Mineral Liberation Characteristics

The degree of liberation of the minerals directly affects the subsequent flotation performance, and, in order to further understand the liberation characteristics of the main valuable minerals (magnetite/hematite), primary gangue quartz, and other minerals, their degrees of liberation were analyzed. Figure 4 shows that the 100% mineral liberation of magnetic/hematite, quartz, turquoise, and ankerite are 76.38%, 75.4%, 50.16%, and 66.13%, respectively. In the flotation feed, the mineralogical characterization of the magnetite/hematite particles of 88.66% purity contain 6.58% quartz, while the quartz gangue mineral particles of 93.34% purity consists of 4.79% magnetite/hematite (Table II). In addition, 71.83% and 86.24% purity of turquoise and ankerite contain 16.33% and 5.22% magnetite/hematite in addition to 5.88% and 3.11% quartz, respectively (Table II). It is worth mentioning that

Table I. Mineral quantitative analysis results of flotation feed

Mineral Name	Magnetite/ hematite	Quartz	Chlorite	Ankerite	Illite	Pyroxferroite	Calcite	Ferrohypersthene
(Wt.%)	62.99	29.97	2.55	1.48	0.72	0.35	0.35	0.18
Mineral	Oligoclase	Pyrite	Apatite	Dolomite	Orthoclase	Siderite	Other	Total
(Wt.%)	0.15	0.14	0.12	0.11	0.11	0.03	0.75	100.00

the liberation degree of magnetite/hematite and quartz particles in addition to siderite particles (if they exist) significantly impacts the separation performance, whereas the liberation degree of the other minerals may not significantly impact the separation performance.

The AMICS with hybrid mode options of backscattered electrons for mineral map images shown in Fig. 5 indicates the advanced particle segmentation of magnetic/hematite, quartz, turquoise, ankerite, and other minerals. It confirms that the main minerals are not fully liberated, and that the turquoise mineral liberation is the lowest in comparison to the other minerals, and both magnetite/hematite and quartz have almost the same degrees of liberation of 76.38% and 75.4%, respectively.

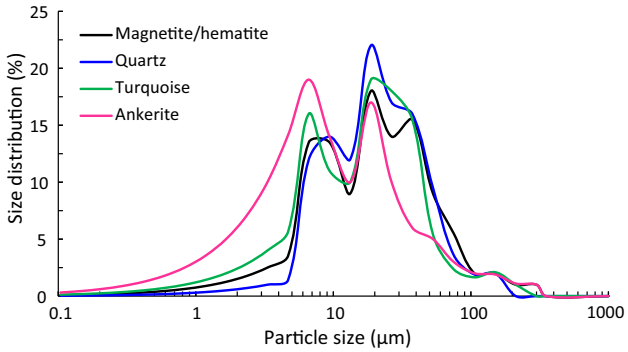

Fig. 3. Particle size analysis of main minerals.

Two-Step Flotation Circuit

In the two-step flotation process (Fig. 6), direct flotation experiments as an open circuit were conducted using 0.8 kg/t starch and 0.2 kg/t TD-II collector to float siderite at near-neutral pH. Then, reverse flotation as both open and closed circuits at 11.5 pH was conducted at the roughing stage using 0.5 kg/t starch, 0.8 kg/t calcium oxide, and 0.4 kg/t TD-II collector, while at the cleaning stage, 0.4 kg/t TD-II collector was used. The pH was adjusted to pH 11.5 for each scavenging step, and the results in the case of open circuit reverse flotation are shown in Table III, clearly indicating that the final yield and grade of 44.53% and 66.28%, respectively, with 64.90% recovery were obtained.

Using a closed circuit in the reverse flotation stage in the same operation conditions mentioned in the open circuit process and shown in Fig. 6, the circuit becomes complicated, and a circuit analysis simulation method such as nodal analysis was conducted.

Using nodal analysis, the circuit was reduced to simple nodes, as shown in Fig. 7, which also shows that there are 10 nodes and 17 streams. The nodes are classified into either a separator or a junction based on the number of input and output streams. Thus, nodes 1, 4, 5, 7, 8, and 10 are separators, while nodes 2, 3, 6, and 9 are junctions. The characteristics of the streams entering and exiting a node are identified by the connection matrix, Ci,j, for node i and stream j, as shown in Fig. 8. From the sum of each column in Fig. 8, there are 1 feed (+ 1), 3 products (– 1), and 13 internal (0) streams in the

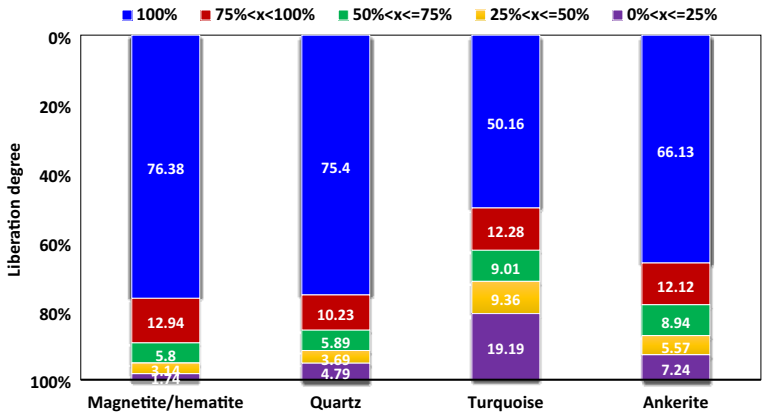

Fig. 4. Degree of the liberation of main minerals in the flotation feed.

Table II. Mineralogical characterization of the main minerals in the flotation feed

Mineral	Magnetite/hematite	Quartz	Turquoise	Ankerite	Others	Total
Contents	88.66	6.58	2.37	0.27	2.12	100
	4.79	93.34	0.56	0.11	1.2	100
	16.33	5.88	71.83	1.05	4.91	100
	5.22	3.11	0.58	86.24	4.85	100

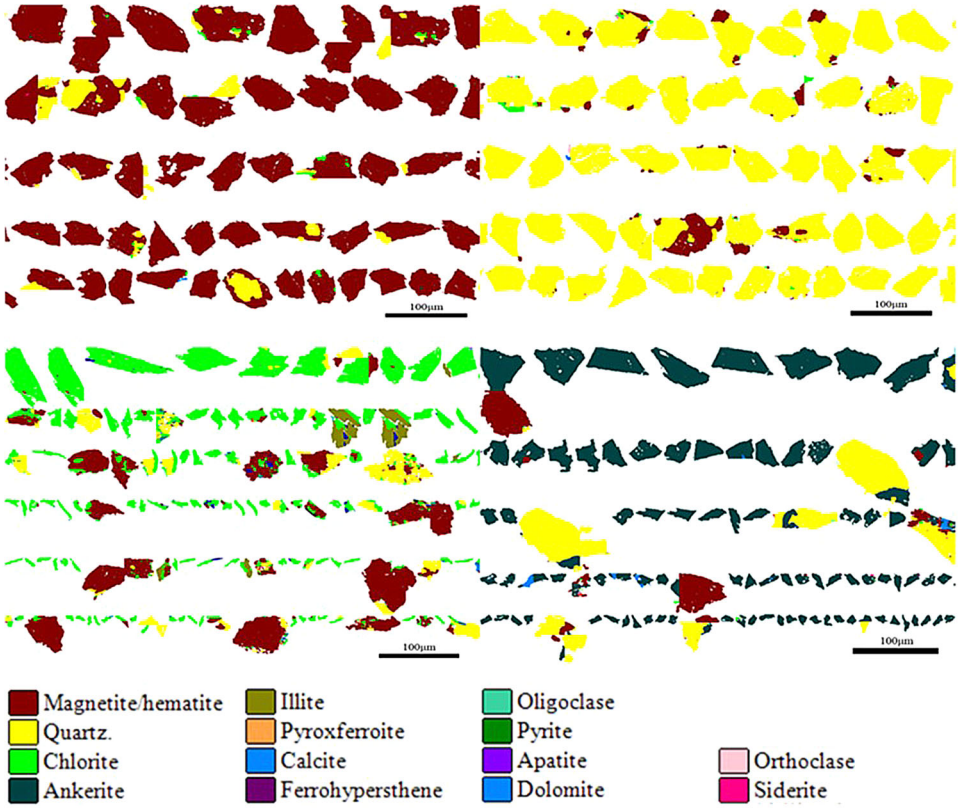

Fig. 5. AMICS images of the mineral map after particle mode analysis of the flotation feed sample.

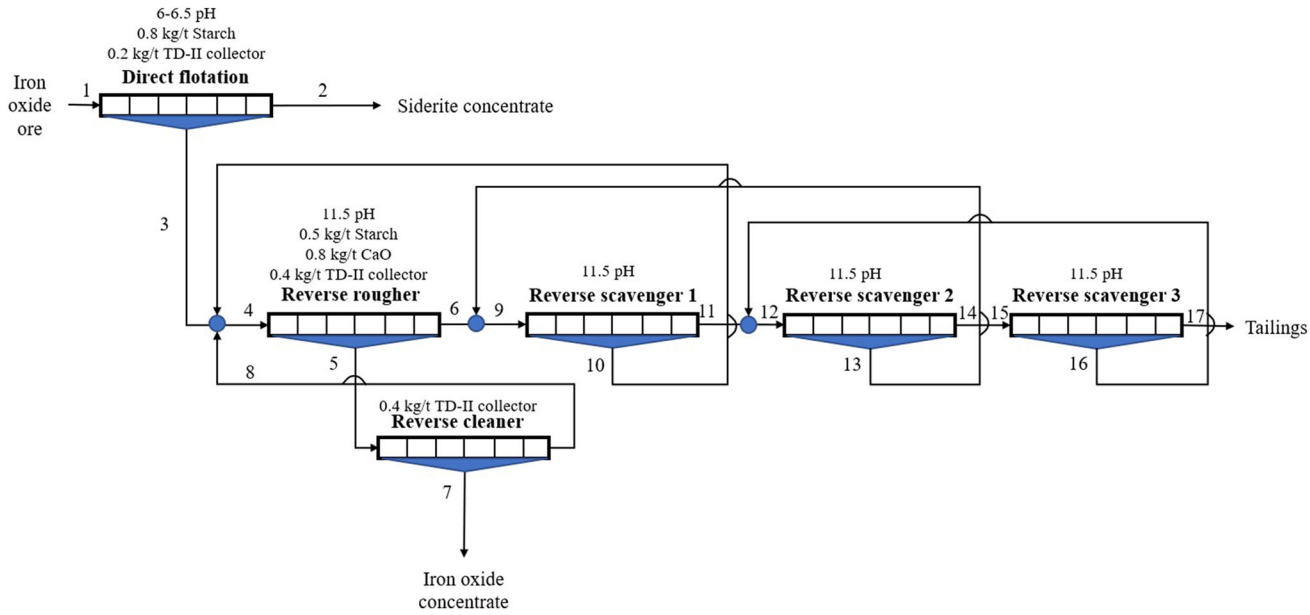

Fig. 6. Flowchart of two-step flotation process.

circuit, while, from the sum of each row in Fig. 8, there are 4 junctions (+ 1) and 6 separators (– 1) in the circuit.

In addition to both the material matrix $M_{1,j}$ of the weight percentages (Eq. 5) and the component matrix $A_{i,j}$ (Eq. 6) of the total iron grade around a node, a set of linear equations was established. For node 1, for example:

$$M_{1,j} = B_1 - B_2 - B_3 \tag{5}$$

$$A_{1,j} = B_1 a_1 - B_2 a_2 - B_3 a_3 \tag{6}$$

Table III. Results of the open circuit two-step flotation process

Stream #	Stream name	Yield (%)	Total Fe grade (%)	Total Fe recovery (%)
1	Circuit feed	100.00	45.48	100.00
2	Siderite concentrate	10.61	43.22	9.72
8	Circuit concentrate	**44.53**	**66.28**	**64.90**
11	Scavenger 1 sink	5.43	44.43	5.30
14	Scavenger 2 sink	3.42	33.23	2.50
16	Scavenger 3 sink	3.11	23.79	1.63
17	Circuit tailing	32.90	22.05	15.95

Bold values indicate the final concentrate which is the most important product from the processing circuit

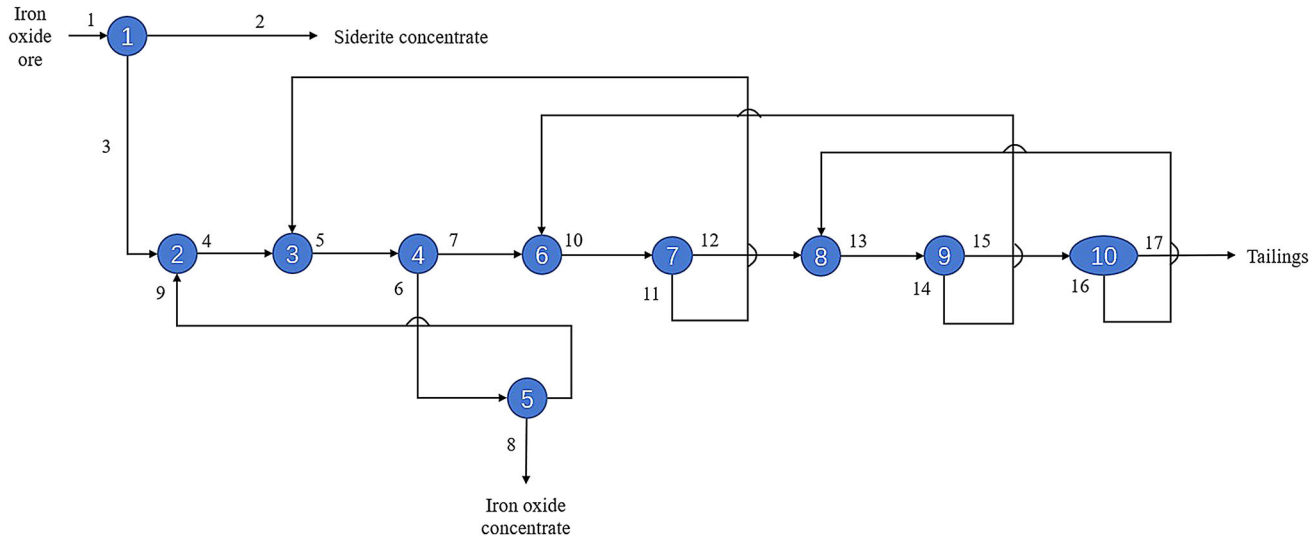

Fig. 7. Nodal form of the two-step flotation process flowsheet.

$$C_{i,j} = \begin{vmatrix} 1 & -1 & -1 & 0 & 0 & 0 & 0 & 0 & 0 & 0 & 0 & 0 & 0 & 0 & 0 & 0 & 0 \\ 0 & 0 & 1 & -1 & 0 & 0 & 0 & 0 & 1 & 0 & 0 & 0 & 0 & 0 & 0 & 0 & 0 \\ 0 & 0 & 0 & 1 & -1 & 0 & 0 & 0 & 0 & 0 & 1 & 0 & 0 & 0 & 0 & 0 & 0 \\ 0 & 0 & 0 & 0 & 1 & -1 & -1 & 0 & 0 & 0 & 0 & 0 & 0 & 0 & 0 & 0 & 0 \\ 0 & 0 & 0 & 0 & 0 & 1 & 0 & -1 & -1 & 0 & 0 & 0 & 0 & 0 & 0 & 0 & 0 \\ 0 & 0 & 0 & 0 & 0 & 0 & 1 & 0 & 0 & -1 & 0 & 0 & 0 & 1 & 0 & 0 & 0 \\ 0 & 0 & 0 & 0 & 0 & 0 & 0 & 0 & 0 & 1 & -1 & -1 & 0 & 0 & 0 & 0 & 0 \\ 0 & 0 & 0 & 0 & 0 & 0 & 0 & 0 & 0 & 0 & 1 & -1 & 0 & 0 & 0 & 1 & 0 \\ 0 & 0 & 0 & 0 & 0 & 0 & 0 & 0 & 0 & 0 & 0 & 0 & 1 & -1 & -1 & 0 & 0 \\ 0 & 0 & 0 & 0 & 0 & 0 & 0 & 0 & 0 & 0 & 0 & 0 & 0 & 0 & 1 & -1 & -1 \end{vmatrix}$$

Fig. 8. Connection matrix of the two-step flotation process.

By using Gaussian elimination, the mass flow rate for each stream was determined, which is achieved by knowing the Fe assay of 13 streams for the circuit having 1 feed stream and 6 separators. The process streams that were sampled and analyzed for the complete circuit balancing, and to estimate the unknown mass flows, were the circuit feed and product streams (1, 2, 8, and 17) in addition to internal stream numbers 3, 6, 7, 9, 11, 12, 14, 15, and 16. The total Fe% of the selected streams 1, 2, 3, 6, 7, 8, 9, 11, 12, 14, 15, 16, and 17 were 44.82%, 38.52%, 45.46%, 63.25%, 24.95%, 65.03%, 46.82%, 49.77%, 23.38%, 33.34%, 22.88%, 28.40%, and 22.62%, respectively. By using Gaussian elimination for the nodal analysis method, the

complete results of the circuit balancing are shown in Table IV. The yield, grade, and recovery of the concentrate stream (stream 8) were 48.92%, 65.03%, and 70.98%, respectively.

Reverse Flotation Circuit

The suggested flotation process conditions based on an extensive investigation in a previous work by the authors[15] are 11.5 pH, 1 kg/t of starch for hematite/magnetite depression, 0.3 kg/t of calcium oxide for quartz activation, and 0.4 kg/t of TD-II for quartz flotation in the roughing flotation step, then 0.3 kg/t of TD-II at pH 11.5 was used in the cleaning flotation step, while the three scavenging steps were carried out at 11.5 pH.

Similar to the two-step flotation process, the reverse flotation process was performed as open and closed-circuits (Fig. 9). In the case of an open circuit, yield, grade, and recovery values of the final concentrate are 32.15%, 65.63%, and 47.39%, respectively, as shown in Table V.

The nodal analysis of the closed circuit process test carried out under the same conditions simplified the processing circuit shown in Fig. 9 into a nodal form, as shown in Fig. 10. Compared to the two-step flotation circuit, Fig. 10 for the reverse flotation circuit shows that the number of nodes and streams were reduced to 9 and 15, respectively. Thus, the flotation circuit was simplified to fewer flotation units and streams. The connection matrix

Table IV. Nodal analysis results of the two-step flotation process

Stream #	Stream name	Yield (%)	Total Fe grade (%)	Total Fe recovery (%)
1	Circuit feed	100.00	44.82	100.00
2	Siderite concentrate	9.22	38.52	7.93
3	Direct flotation sink	90.78	45.46	92.07
4	Junction 2 out	96.08	45.54	97.61
5	Rougher feed	100.02	45.70	101.99
6	Rougher sink	54.22	63.25	76.52
7	Rougher float	47.06	24.95	26.20
8	Circuit concentrate	**48.92**	**65.03**	**70.98**
9	Cleaner float	5.30	46.82	5.54
10	Scavenger 1 feed	50.08	25.46	28.44
11	Scavenger 1 sink	3.94	49.77	4.38
12	Scavenger 1 float	46.14	23.38	24.07
13	Scavenger 2 feed	48.12	23.59	25.32
14	Scavenger 2 sink	3.02	33.34	2.25
15	Scavenger 2 float	43.95	22.88	22.44
16	Scavenger 3 sink	1.98	28.40	1.25
17	Circuit tailing	41.97	22.62	21.18

Bold values indicate the final concentrate which is the most important product from the processing circuit

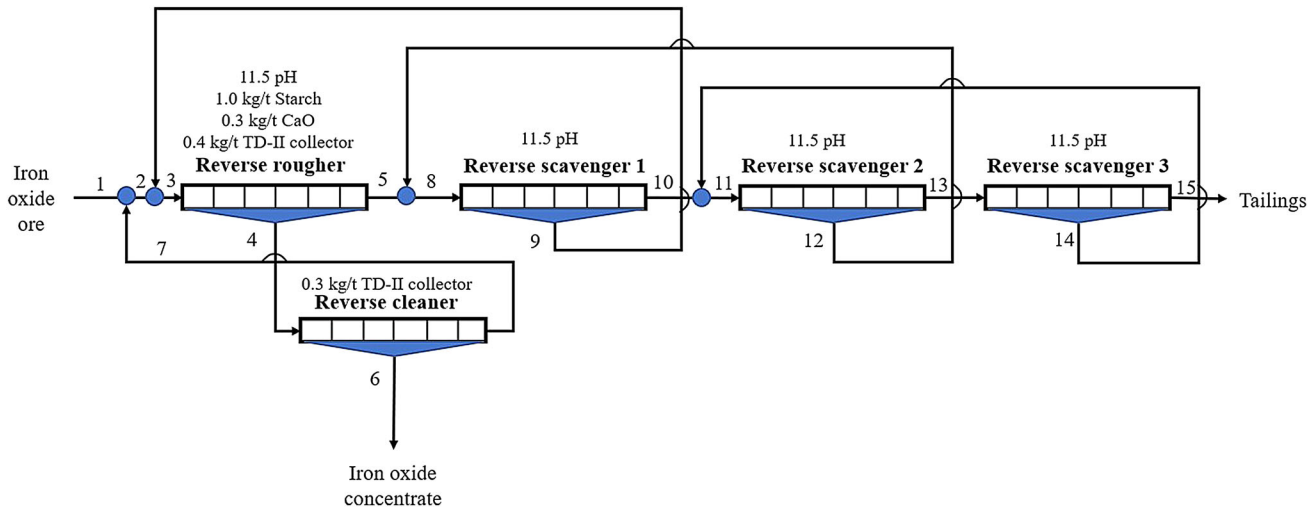

Fig. 9. Flowchart of the reverse flotation process.

Table V. Open circuit results of the reverse flotation process

Stream #	Stream name	Yield (%)	Total Fe grade (%)	Total Fe recovery (%)
1	Circuit feed	100.00	44.53	100.00
6	Circuit concentrate	**32.15**	**65.63**	**47.39**
9	Scavenger 1 sink	7.19	51.23	8.27
12	Scavenger 2 sink	3.50	43.68	3.44
14	Scavenger 3 sink	3.50	37.03	2.88
15	Circuit tailing	53.70	31.54	38.03

Bold values indicate the final concentrate which is the most important product from the processing circuit

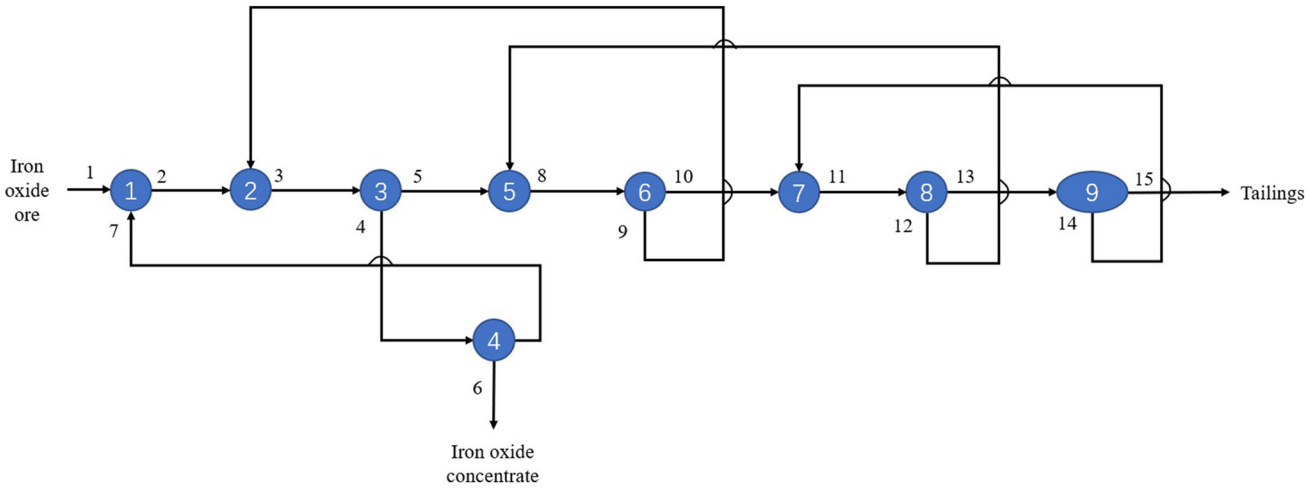

Fig. 10. Nodal form of the reverse flotation process flowsheet.

$$C_{i,j} = \begin{vmatrix} 1 & -1 & 0 & 0 & 0 & 0 & 1 & 0 & 0 & 0 & 0 & 0 & 0 & 0 & 0 \\ 0 & 1 & -1 & 0 & 0 & 0 & 0 & 0 & 1 & 0 & 0 & 0 & 0 & 0 & 0 \\ 0 & 0 & 1 & -1 & -1 & 0 & 0 & 0 & 0 & 0 & 0 & 0 & 0 & 0 & 0 \\ 0 & 0 & 0 & 1 & 0 & -1 & -1 & 0 & 0 & 0 & 0 & 0 & 0 & 0 & 0 \\ 0 & 0 & 0 & 0 & 1 & 0 & 0 & -1 & 0 & 0 & 0 & 1 & 0 & 0 & 0 \\ 0 & 0 & 0 & 0 & 0 & 0 & 0 & 1 & -1 & -1 & 0 & 0 & 0 & 0 & 0 \\ 0 & 0 & 0 & 0 & 0 & 0 & 0 & 0 & 1 & -1 & 0 & 0 & 0 & 1 & 0 \\ 0 & 0 & 0 & 0 & 0 & 0 & 0 & 0 & 0 & 0 & 1 & -1 & -1 & 0 & 0 \\ 0 & 0 & 0 & 0 & 0 & 0 & 0 & 0 & 0 & 0 & 0 & 0 & 1 & -1 & -1 \end{vmatrix}$$

Fig. 11. Connection matrix of the reverse flotation process.

for the reverse flotation circuit is shown in Fig. 11. From the sum of each column shown in Fig. 11, there are 1 feed, 2 products, and 12 internal streams in the circuit, while, from the sum of each row, there are 5 separators and 4 junctions.

The minimum number of streams needed to be analyzed for the complete nodal analysis method of the reverse flotation process consisting of 1 feed and 5 separators is 11. Thus, the selected streams were 1, 4, 5, 6, 7, 9, 10, 12, 13, 14, and 15, and their total Fe% assays were 44.74%, 55.96%, 36.72%, 65.22%, 37.78%, 48.08%, 29.85%, 48.16%, 27.48%, 47.26%, and 24.70%, respectively. The complete results of the reverse flotation circuit are shown in Table VI. The final concentrate yield, grade, and recovery are 49.45%, 65.22%, and 72.09%, respectively.

Table VI. Nodal analysis results of the reverse flotation process

Stream #	Stream name	Yield (%)	Total Fe grade (%)	Total Fe recovery (%)
1	Circuit feed	100.00	44.74	100.00
2	Junction 1 out	125.20	43.34	121.28
3	Rougher feed	178.68	44.76	178.75
4	Rougher sink	74.65	55.96	93.37
5	Rougher float	104.03	36.72	85.38
6	Circuit concentrate	**49.46**	**65.22**	**72.10**
7	Cleaner float	25.20	37.78	21.28
8	Scavenger 1 feed	0.00	0.00	0.00
9	Scavenger 1 sink	53.48	48.08	57.47
10	Scavenger 1 float	64.76	29.85	43.21
11	Scavenger 2 feed	71.85	31.57	50.69
12	Scavenger 2 sink	14.21	48.16	15.30
13	Scavenger 2 float	57.64	27.48	35.40
14	Scavenger 3 sink	7.09	47.26	7.49
15	Circuit tailing	50.55	24.70	27.91

Bold values indicate the final concentrate which is the most important product from the processing circuit

Table VII. Two-step and reverse flotation circuit

Process	Stream name	Yield (%)	Total Fe grade (%)	Total Fe recovery (%)
Two-step flotation circuit	Circuit concentrate	48.92	65.03	70.98
	Circuit tailing	41.97	22.62	21.18
	Circuit feed	100.00	44.82	100.00
Reverse flotation circuit	Circuit concentrate	49.46	65.22	72.10
	Circuit tailing	50.55	24.70	27.91
	Circuit feed	100.00	44.74	100.00
Comparison	Concentrate	+ 0.54	+ 0.19	+ 1.12

Comparison Between Two-Step and Reverse Flotation Circuits

The two-step and reverse flotation results shown in Table VII show that the product quality of the reverse flotation circuit is comparable to the two-step circuit, with 0.54% higher yield, 0.19% higher grade, and 1.12% higher recovery, besides reducing the reagent consumptions by 0.3 kg/t starch, 0.5 kg/t calcium oxide, and 0.7 kg/t TD-II, in addition to simplifying the processes circuit.

CONCLUSION

The two-step flotation circuit solves the problem of high iron carbonate content in the flotation feed of the largest producer of iron oxide product/concentrate in China, the Donganshan processing plant. However, with the mine development, and for the current analysis, the presence of 0.03% siderite is no longer the main mineral affecting flotation performance, and the main minerals that affect the performance of removing quartz from iron oxide minerals are chlorite and ankerite with a low degree of liberation. By investigating both two-step flotation and reverse flotation circuits as open and closed circuits, and by utilizing the nodal analysis simulation method, the reverse flotation closed-circuit had greater advantages by simplifying the process, improving the separation performance, and minimizing the reagent consumption.

DATA AVAILABILITY

The datasets generated and/or analyzed during the current study are not publicly available due to institutional roles and confidential conditions but are available from the corresponding author on reasonable request.

CONFLICT OF INTEREST

The authors have no competing interests to declare that are relevant to the content of this article.

REFERENCES

1. A. Pattanaik, and R. Venugopal, *Colloid Interface Sci. Commun.* 25, 41 (2018).
2. H. Li, Z. Zhang, L. Li, Z. Zhang, J. Chen, and T. Yao, *Ore Geol. Rev.* 57, 264 (2014).

3. R3: Seven countries with the largest iron ore reserves in the world in 2019 [WWW Document], n.d. https://www.nsenergybusiness.com/features/world-iron-ore-reserves-countries/. Accessed2 Jan 2023.
4. Q. Jia, F. Li, and Y. Qu, *Appl. Mech. Mater.* 303–306, 2559 (2013).
5. Y. Zhao, C. Feng, and D. Li, *Acta Geologica Sin. English Edn.* 88, 1895 (2014).
6. D. Li, W. Yin, J. Yao, A. Ji, J. Xue, and Y. Fu, Jinshu Kuangshan/Metal Mine 51 (2016). https://www.researchgate.net/publication/312372725_Classification_Flotation_of_Donganshan_Siderite-containing_Hematite_Ore.
7. L. Li, W. Yin, D. Feng, and B. Zhang, *Adv. Mat. Res.* 455–456, 91 (2012).
8. S. Montes, and G. Montes Atenas, *Miner. Eng.* 18, 1032 (2005).
9. W.Z. Yin, Y.X. Han, and F. Xie, *J. Cent. S Univ. Technol.* 2010(17), 750 (2010).
10. X. Zhang, X. Gu, Y. Han, N. Parra-Álvarez, V. Claremboux, and S.K. Kawatra, *Miner. Process. Extr. Metall. Rev.* 42, 184 (2019).
11. G. Fan, L. Wang, Y. Cao, and C. Li, *Minerals* https://doi.org/10.3390/min10080681 (2020).
12. L.O. Filippov, K. Silva, A. Piçarra, N. Lima, I. Santos, L. Bicalho, I.V. Filippova, and A.E.C. Peres, *Minerals* 11, 699 (2021).
13. K. Silva, L.O. Filippov, A. Piçarra, I.V. Flilippova, N. Lima, A. Skliar, L. Faustino, and L.L. Filho, *Miner. Eng.* 170, 107004 (2021).
14. Y. Hou, A. Sobhy, and Y. Wang, *Physicochem. Probl. Miner. Process.* 57, 284 (2020).
15. Y. Hou, and A. Sobhy, *Physicochem. Probl. Miner. Process.* 58, 37 (2021).
16. D. Tao, Z. Wu, and A. Sobhy, *Powder Technol.* 379, 12 (2021).
17. A. Sobhy, Z. Wu, and D. Tao, *Miner. Eng.* 163, 106799 (2021).
18. D. Zhang, and X. Gao, *J. Manuf. Syst.* 63, 238 (2022).